LAWRENCE
LIVERMORE
NATIONAL
LABORATORY

UCRL-TR-228327

Persistent Monitoring Platforms Final Report

C.L. Bennett

February 26, 2007

This work was performed under the auspices of the U.S. Department of Energy by University of California, Lawrence Livermore National Laboratory under Contract W-7405-Eng-48.

Persistent Monitoring Platforms

Final Report

LDRD Project Tracking Code: 03-ERD-076

Charles L. Bennett, Principal Investigator

Lawrence Livermore National Laboratory, Livermore, CA 94550

Abstract

This project was inspired and motivated by the need to provide better platforms for persistent surveillance. In the years since the inception of this work, the need for persistence of surveillance platforms has become even more widely appreciated, both within the defense community and the intelligence community. One of the most demanding technical requirements for such a platform involves the power plant and energy storage system, and this project concentrated almost exclusively on the technology associated with this system for a solar powered, high altitude, unmanned aircraft. An important realization for the feasibility of such solar powered aircraft, made at the outset of this project, was that thermal energy may be stored with higher specific energy density than for any other known practical form of rechargeable energy storage. This approach has proved to be extraordinarily fruitful, and a large number of spin-off applications of this technology were developed in the course of this project.

Table of Contents

I. Introduction

Recent world events have made it clearer than ever that there is a substantial need to improve our capability to be able to observe, on a nearly continuous basis, specific regions of the globe that are of high strategic interest. Reconnaissance satellites are fundamentally limited by Keplerian dynamics to approximately 90 minute periods for low earth orbit, and thus very limited access to any given spot on the earth, or for geo-stationary orbits, to the extremely long range of 36 Mm. In neither extreme are satellites well suited to the task of continuously observing events on a fine scale.

On the other hand, aircraft are quite capable of supporting any number of types of sensors, and are quite flexible in terms of vantage point. However, currently available aircraft are severely limited by logistics. Absent mid-air refueling, currently available aircraft have dwell times limited to durations measured in hours.

Solar energy has many characteristics that are very favorable for the purposes of powering a high altitude long endurance (HALE) aircraft. At sufficiently high altitude, above the clouds, sun-light is a highly reliable, highly predictable, renewable energy resource. The primary technical challenge is to be able to store sufficient energy accumulated during the day that overnight flight is enabled. It is this challenge that was addressed and met in the course of the work of this project.

II. Persistent Aircraft Requirement Study

At the foundation of this project is the question of the energy storage and power requirements for the various possible options for persistent aircraft. A basic trade involves the advantages and disadvantages of lighter-than-air vs. heavier-than-air craft. High altitude, lighter-than-air craft are necessarily relatively large. Although no power is required for propulsion of a lighter-than-air in the absence of wind, in fact the winds expected at high altitude are quite significant and need to be considered.

A. Vertical Profile of Mean Winds

An example of the vertical profile of mean wind speed at a fixed location is shown in the figure below, taken from the Sanswire web-site[1].

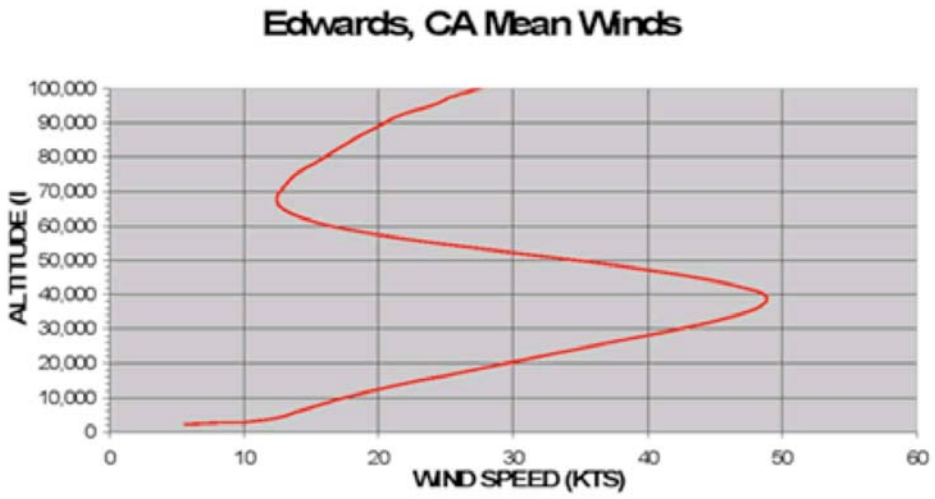

Figure 1. Mean wind speed vs. altitude.

This figure illustrates that winds in the troposphere have a substantial peak as a function of altitude. Since the propulsive power required varies as the cube of an aircraft's airspeed, it is thus highly desirable, in order to minimize the propulsive requirements, to be near the top of the troposphere, where a local minimum in mean wind speed is found.

B. Upper Altitude Wind Speed Statistics

As an estimate of the winds seen by high-altitude aircraft, some measures of the statistical distribution of the wind speeds observed from the global distribution of radiosonde observations[2], as compiled by UKMO, the United Kingdom Meterological Office, for 2001 were computed. The wind speed percentiles (in m/s units) vs. pressure (closely related to altitude) are listed in the table below.

Table 1. High altitude wind speed statistics

Pressure -> Percentile	68 mb	46 mb	32 mb	22 mb	14 mb	10 mb	6.8 mb
50%	8.4(m/s)	9.1	11.6	13.1	13.3	13.8	14.6
90%	26.6	28.6	33.3	37.3	41.6	46.0	50.5
95%	36.7	41.6	47.8	54.1	59.7	64.6	68.5
99%	54.1	61.5	69.0	75.5	84.3	86.2	90.2

For example, for the 68 mb pressure level, approximately 1% of the time, a wind speed of 54 m/s is exceeded. A rough approximation to the probability

distribution vs. speed is given by a simple exponential decline with speed. An example of this approximate probability distribution for the 68 mb pressure level case (corresponding to an approximate altitude of 19 km) is shown in the figure below.

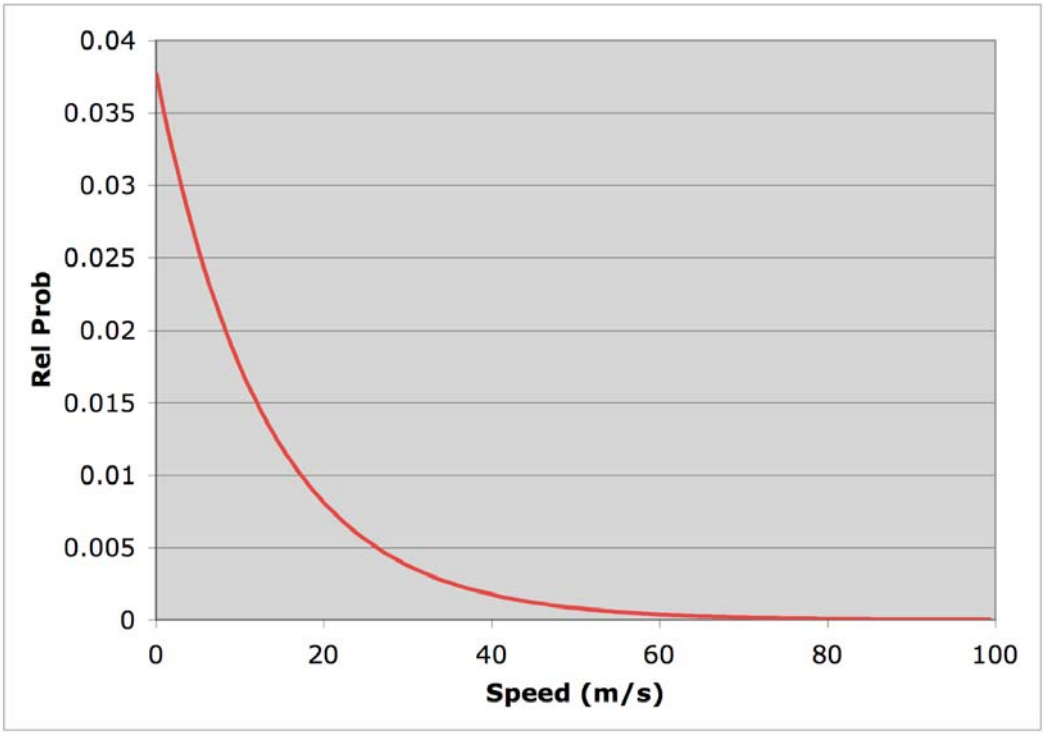

Figure 2. The approximate probability distribution for the global distribution of wind-speed at a pressure level of 68 mb derived from the UKMO observations in 2001 is plotted as a function of speed.

From this curve, the following weighted means are found:

$$
\begin{aligned}
&< U >= 12.7 \frac{m}{s} \\
&\sqrt{< U^2 >} = 18.0 \frac{m}{s} \\
&< U^3 >^{1/3} = 23.0 \frac{m}{s}
\end{aligned}
\tag{1}
$$

It is found that the global probability distributions of wind speed at high altitude are very similar in shape to the curve shown in figure 2. Thus, it is notable that the cube root of the mean cube wind speed is approximately double the mean wind speed, as in the example shown in expression 1 above.

C. Upper Altitude Wind Dynamics

In the animation below, a movie of the global winds at a pressure level of 200 mb is shown[3]. This clip covers the time interval from September 1 to September 6, 2004 at 3 hour intervals. This illustrates the fact that high winds may be sustained in a given region for several days at a time. In consideration of the cubic sensitivity of the power demands in order to weather such storms, it is clear that bad weather will occasionally require extraordinarily high propulsive power levels to simply maintain station.

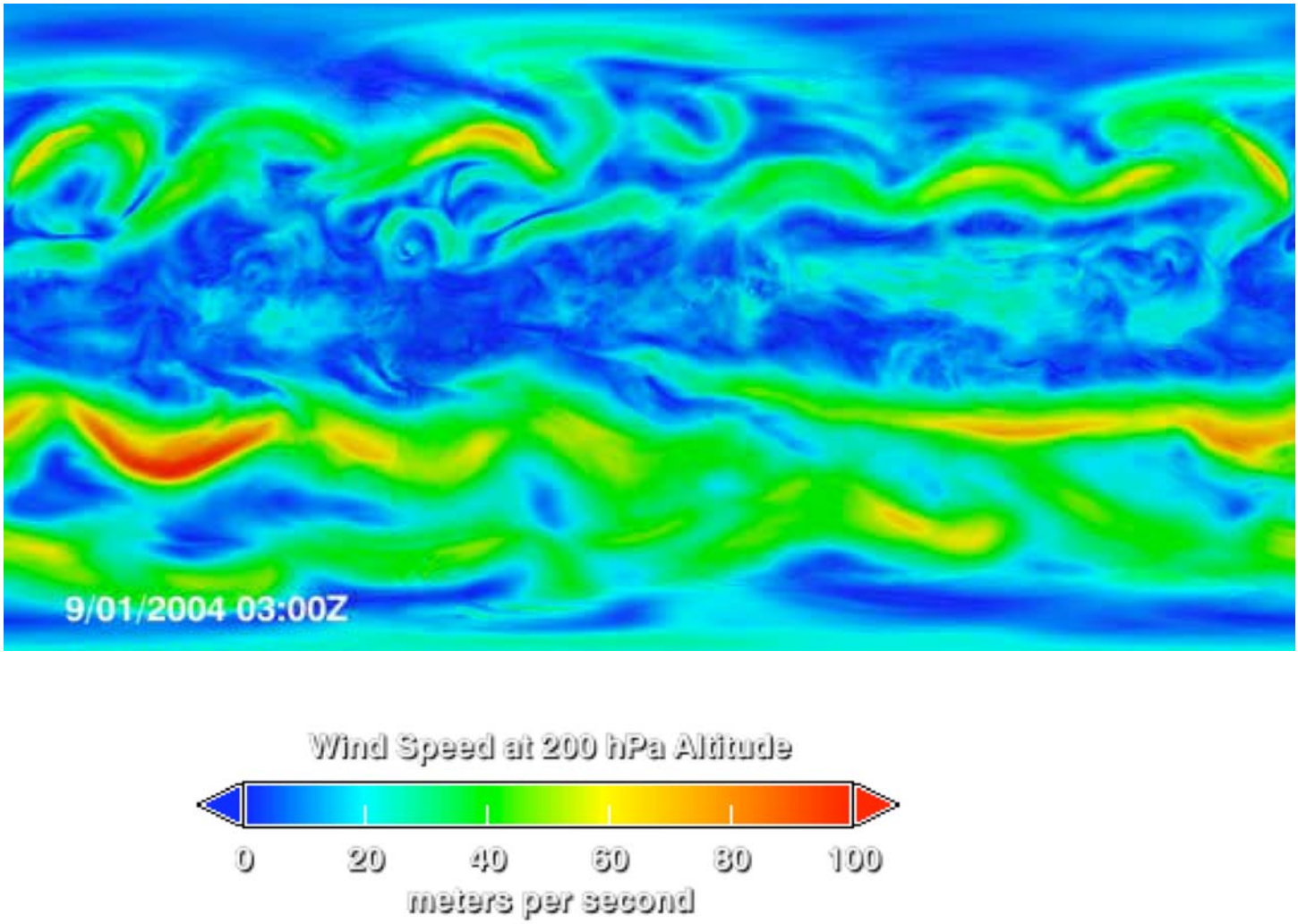

Figure 3. A movie clip displays the global upper altitude wind velocity field for a one week period.

D. Station Keeping Aerodynamics

At a minimum, in order to maintain a fixed position with respect to the ground in the face of a wind speed U(m/s), the thrust force D, that must be supplied is determined by the coefficient of drag C_D and a reference area A as follows.

$$D = C_D \frac{1}{2} \rho U^2 A \tag{2}$$

For heavier-than-air craft, the reference area is generally taken to be the area of the wing, while for lighter-than-air craft, the reference area is here defined as the 2/3 power of the aircraft volume. The thrust power per unit reference area is then

$$\frac{P_{thrust}}{A} = C_D \frac{1}{2} \rho U^3 \tag{3}$$

There is a fundamental dichotomy in the power plant requirements for heavier-than-air vs. lighter-than-air craft. Obviously, a lighter-than-air craft has no need to supply power to keep itself aloft. However, in order to maintain station with respect to a particular position on the ground, it must be apply to provide sufficient power to keep its instantaneous air velocity vector opposite in direction, and equal in magnitude, to the local wind velocity. In view of the cubic relation between thrust power and airspeed in expression 3 above, the mean power required of an airship power plant is proportional to the weighted average of the cube of the wind speed. In contrast, a heavier-than-air craft must continually fly at sufficient speed to keep itself aloft.

1. Airship Station Keeping

According to Lutz and Wagner[4], carefully designed forms for airships may have quite low coefficients of drag. A plot from their article is reproduced in figure 4 below. It can be seen that, for a reasonably broad range of Reynolds numbers, the drag coefficient may be less than 1%. An example of the Airship profile for the lowest Reynolds number range, "regime I", is shown in figure 5. Thus, from expression 3 above, the thrust power density for a robust airship (capable of withstanding the 99th percentile winds) may be quantified as follows, assuming a drag coefficient of 0.01.

$$\frac{P_{thrust}}{A}(20\text{km}, 99\%\text{wind}) \approx 70\frac{W}{m^2} \quad , \qquad \frac{P_{thrust}}{A}(30\text{km}, 99\%\text{wind}) \approx 50\frac{W}{m^2} \qquad (4)$$

The case associated with 90th percentile winds is quite a bit less demanding.

$$\frac{P_{thrust}}{A}(20\text{km}, 90\%\text{wind}) \approx 8\frac{W}{m^2} \quad , \qquad \frac{P_{thrust}}{A}(30\text{km}, 90\%\text{wind}) \approx 7\frac{W}{m^2} \qquad (5)$$

From this example, it can be observed that the thrust power relative to reference area is relatively insensitive to altitude, but is extremely sensitive to the local wind speed. With sufficient energy storage available to supply propulsion to "weather the storms", it is the mean wind speed cubed that sets the requirements for the mean thrust power to reference area ratio. A plot of this mean power density, together with the median wind speed, is shown in figure 6 below.

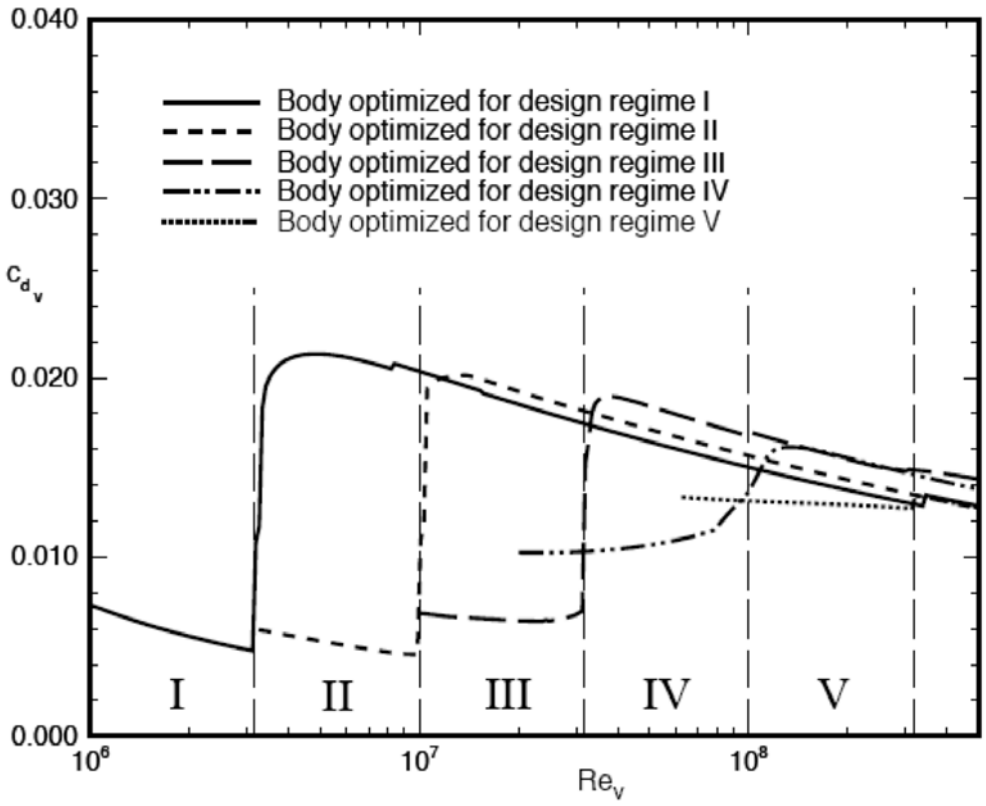

Fig. 4. The drag coefficient for symmetrical airship bodies is shown as a function of Reynolds number for five shapes, each designed for optimal performance in a given range of Re numbers. Here the volumetric drag coefficient is defined by $C_{d_V} = D/(\frac{\rho}{2}U_\infty^2 V^{2/3})$, and the volumetric Reynolds number is defined by $Re_V = \frac{U_\infty V^{1/3}}{\nu}$, with V being the volume of the airship body.

The shape of the airship that corresponds to region I in figure 4 is shown in figure 5 below.

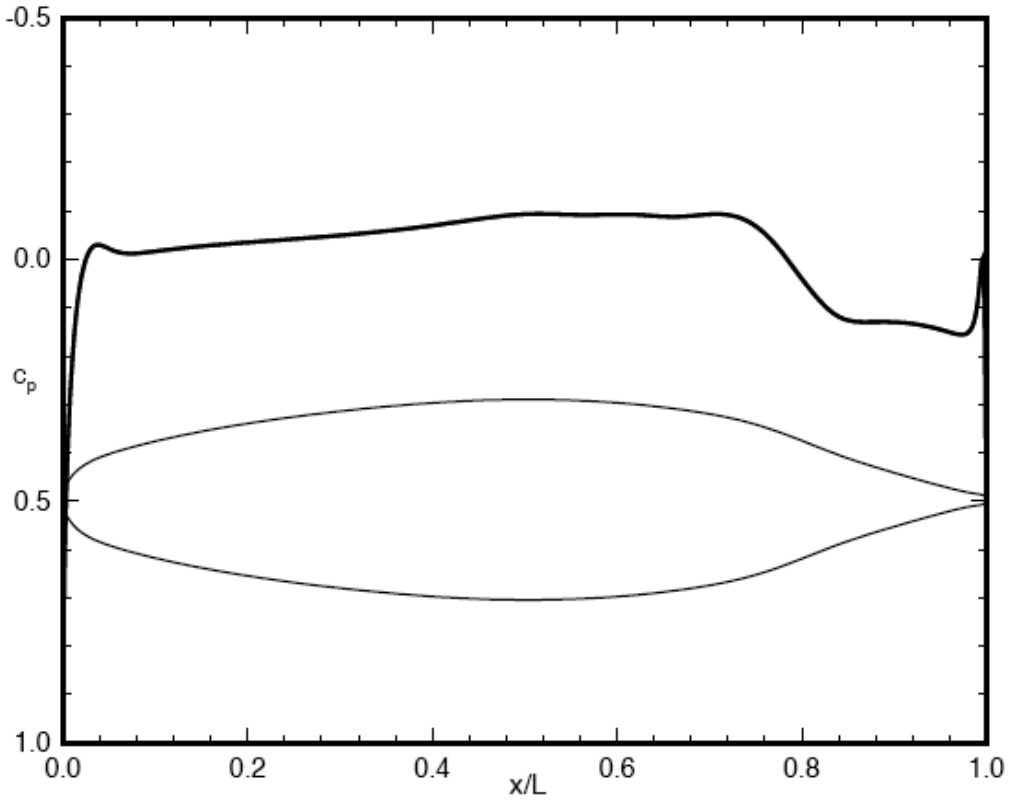

Figure 5. This is a plot of the pressure distribution and profile of an airship taken from the lowest Reynolds number region of Lutz-Wagner.

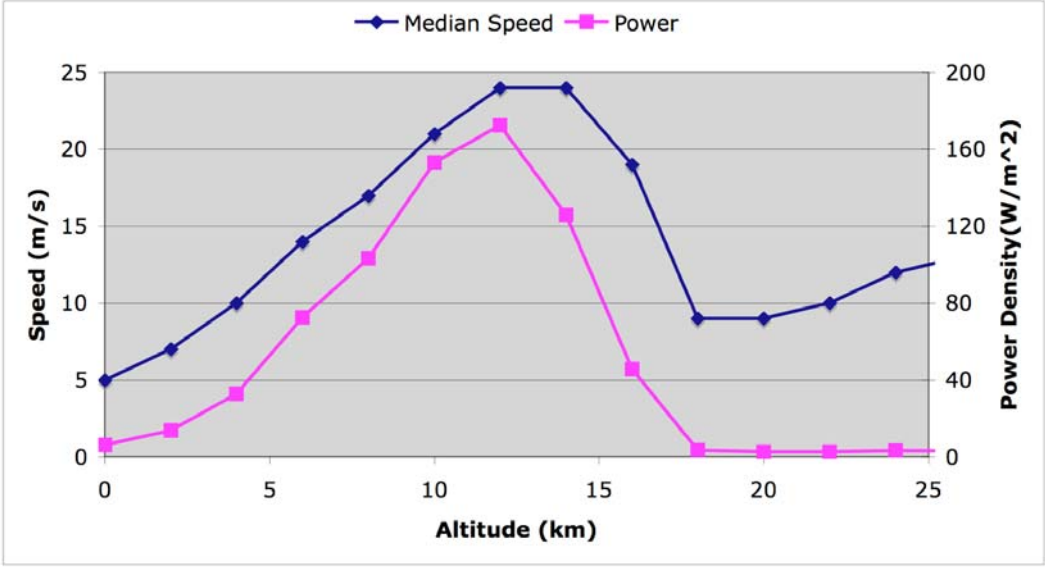

Figure 6. This is a plot of the median windspeed and mean power density required for an airship to maintain station above a fixed position as a function of altitude.

Considering the enormously great variation in the mean thrust power areal density with altitude, it is clear that airships are best deployed above the high speed winds of the troposphere. It is quite interesting to note that the power plant requirements are not very sensitive to altitude, once the aircraft is above the troposphere. The reason for this weak dependence on altitude is that although the mean wind speed continues to increase with altitude, the atmospheric density decreases exponentially, and these two factors tend to approximately compensate each other.

2. Heavier-than-air Craft Station Keeping

For a heavier-than-air craft, the weight of the aircraft must be supported by the lift. For SLUF (Straight and Level Un-accelerated Flight) conditions, the thrust must equal the drag, while the lift must equal the weight. This leads to the following expression for the SLUF speed,

$$U_{SLUF} = \sqrt{\frac{2Mg}{\rho C_L A}} \tag{6}$$

the thrust power to aircraft mass ratio,

$$\frac{P_{thrust}}{M_{aircraft}} = \frac{C_D}{C_L} gV \tag{7}$$

and the thrust power to reference area ratio:

$$\frac{P_{thrust}}{A} = C_D \sqrt{\frac{2}{\rho}} \left(\frac{Mg}{C_L A} \right)^{3/2} \tag{8}$$

Note that both the SLUF speed and the power areal density vary as the inverse square root of the atmospheric density, and thus both increase exponentially with altitude. A plot of the P/A and the SLUF speed is shown in the figure below as a function of altitude.

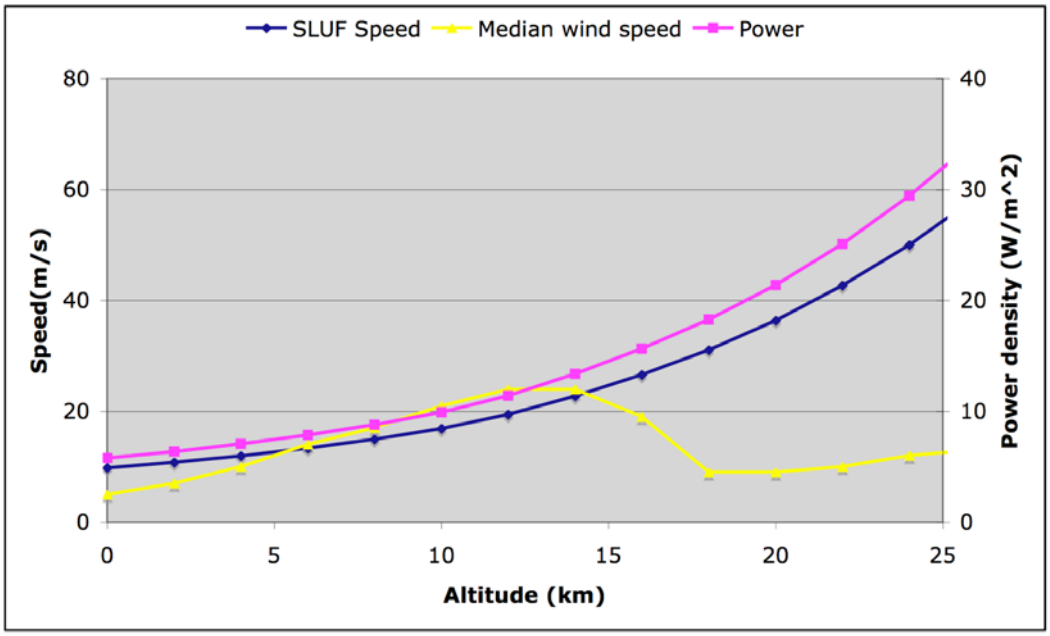

Figure 7. The SLUF speed for an aircraft with a lift coefficient of 0.5 and a drag coefficient of 0.01 is displayed as a function of altitude. The thrust power relative to wing area is also plotted, with the right hand vertical scale. The wing loading assumed for the calculation of these curves is 3 kg/m^2.

For the purpose of maintaining position over an area of interest, the propulsive power requirements are determined by the maximum of either the power needed to overcome the wind speed, or the power needed to maintain SLUF conditions. With this requirement, the power to reference area ratio for heavier-than-air craft is compared with the power to reference area ratio for lighter-than-air craft in the following figure.

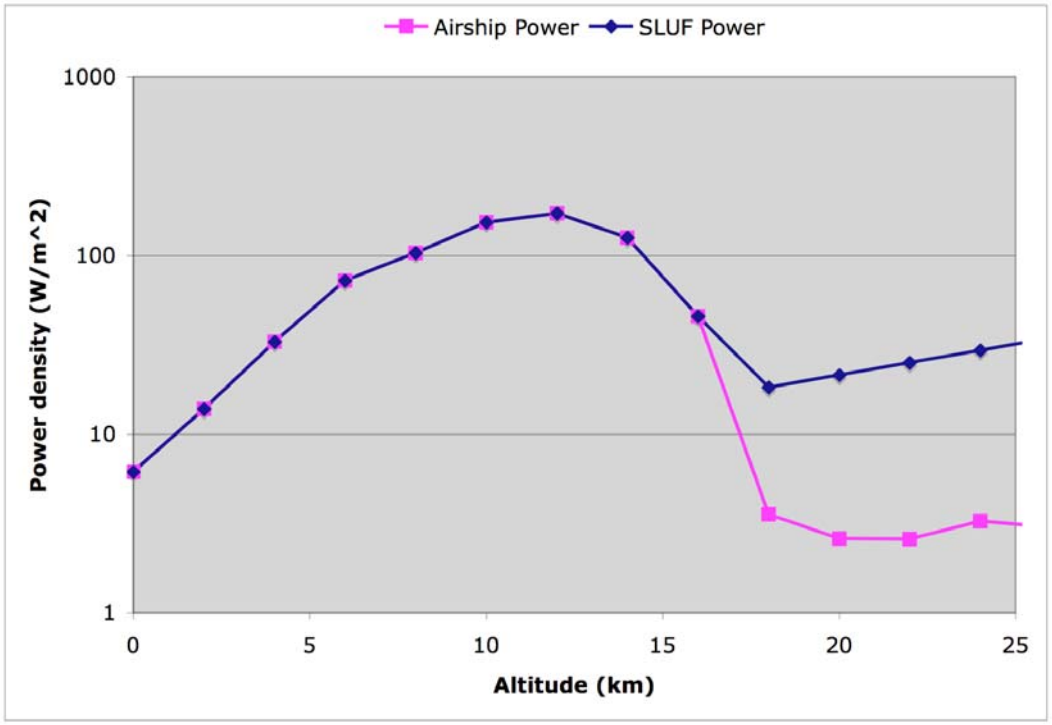

Figure 8. The power to reference area required to maintain station is plotted for lighter-that-air and heavier-than-air craft as a function of altitude. In both cases the drag coefficient is assumed to be 0.01. For the heavier-than-air craft, the lift to drag ratio is 50, and the wing loading is 3 kg/m^2.

As long as the power requirements are dictated by the wind speed, since achievable drag coefficients for both types of aircraft are approximately the same, their power requirements are nearly the same. However, at the top of the troposphere, where the median windspeed is lower, heavier-than-air craft typically require a much larger power density than do lighter-than-air craft.

3. Station Keeping Conclusion

For the purposes of persistent monitoring of a specific region, it is advantageous to have as large a field of regard as possible. Clearly higher altitudes enable a broader coverage region. At higher altitude, however, the air becomes less dense, and a heavier-than-air craft must fly at ever higher speed to remain aloft. We are thus led to a strong technical preference for the lighter-than-air case. Since the power areal density requirement varies only weakly with altitude above the tropopause, there is a great deal of flexibility in the choice of operating altitude, and furthermore, with such high altitudes, persistent monitoring platforms are well above the domain of commercial passenger aircraft. This has a further practical advantage that such platforms can operate in airspace that is not populated by commercial aircraft.

Assuming that an airship of the Lutz-Wagner form is chosen as the vehicle of choice for a persistent platform, and that the volumetric Reynolds number is required to be 10^6 for the operating altitude of choice, then the power per unit of displaced air mass can be computed as a function of altitude. This quantity is plotted in the following figure.

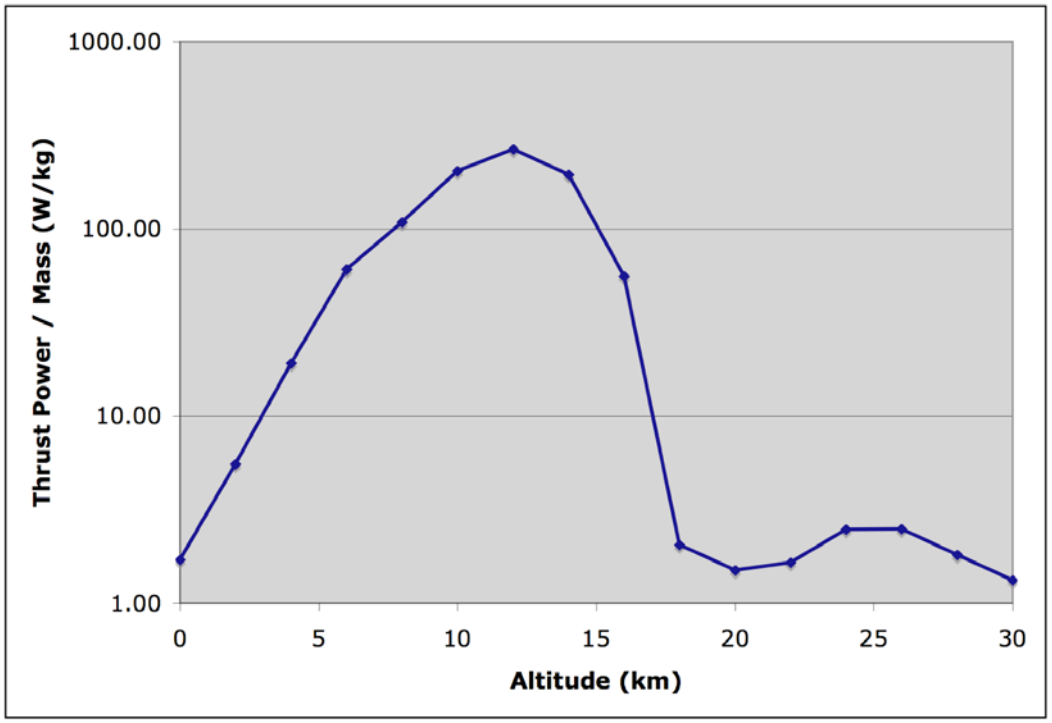

Figure 9. The mean thrust power to displaced airmass ratio is plotted as a function of altitude for a Lutz-Wagner airship capable of maintaining station in the face of upper altitude winds.

For altitudes in the lower stratosphere, the thrust power to displaced air-mass is approximately independent of altitude, and is only a few W/kg. It is interesting, furthermore that there are local minima in the thrust power to displaced airmass ratio at both 20 km, and above 30 km.

E. Energy Storage Requirement

At the very least, for a solar powered aircraft, it is necessary to provide sufficient energy storage to provide the median power demands over the duration of the night. Of course, the length of the night depends not only on season, but on latitude as well. For latitudes outside the arctic, night lasts less than 24 hours. Thus typically 10 to 20 hours worth of power are needed to keep aloft through the diurnal cycle for most seasons and latitudes.

However, as can be seen in the movie clip shown in figure 3 above that illustrates a period of stormy weather, it is not unusual for winds at high altitude to be greater than average for several days at a time. It is thus highly desirable to provide sufficient energy storage to allow station keeping in the face of such storms, and provide at least several days worth of median energy storage, so that at least some ability to weather storms is available.

Since a stratospheric airship requires a few Watts per kg of displaced air mass, the energy storage desired is on the order of a few tens of W-hour per kg of displaced air mass. Since the mass of the energy storage medium can only be a relatively small fraction of the displaced air mass, it is desirable to provide at least several hundred W-hours of stored energy per kg of storage medium mass. This level of specific energy storage is extremely demanding.

III. Energy Storage Alternatives

At the end of the previous section, it was found that the energy storage requirements for solar powered aircraft are quantitatively at the level of at least several hundred W-hours per kg of the energy storage medium mass. This is quite challenging for rechargeable or renewable energy storage technology.

There are a number of alternatives for the storage of energy that can be considered. These include

A. Nuclear
B. Compressed Air
C. Gravitational
D. Rotational Kinetic (flywheels)
E. Super Capacitors
F. Fuel Cells
G. Chemical (batteries)
H. Thermal

In the next few sections, each of these possibilities is briefly discussed

A. Nuclear Energy

Although not a renewable energy storage system, the energy density in nuclear fuel is extremely high. However, it is extremely unlikely that nuclear reactor powered aircraft will be permitted to fly over the earth in the foreseeable future, and this approach is not considered further here.

B. Compressed Air

The storage of energy in the form of compressed air is very limited in specific energy content. For example, for the case of air as the storage medium, and ignoring completely the mass of the pressure vessel, the order of magnitude of the energy storage density is given by

$$E \approx pV$$
$$\frac{E}{M} \approx \frac{p}{\rho} \sim 20 \frac{Wh}{kg} \tag{9}$$

Since the mass of the pressure vessel must also be included, it is clear that compressed gas storage is not competitive with batteries.

C. Gravitational

This storage method is possible with heavier-than-air craft. In this case, obviously the gravitational potential energy is simply given by

$$E = MgH$$
$$\frac{E}{M} = gH = 2.7 \frac{Wh}{kg} H(km) \tag{10}$$

Clearly, this specific energy density, even for a height drop of 10 km, is not high.

D. Flywheels

The specific energy storage density of flywheels is limited by the very high stresses associated with high speed rotation. State of the art[5] flywheels are currently providing approximately only 130 Wh/kg.

E. Super Capacitors

The specific energy storage capacity of state of the art capacitors is quite low[6], at the level of 3 to 5 Wh/kg.

F. Fuel Cells

The URFC (Unitized Recombinant Fuel Cell) energy storage method is based on the dissociation of water by electrolysis as the charging mechanism, with storage of the hydrogen and oxygen for the later production of electrical power by combination in the fuel cell. This technology does not yet appear to be very mature, but has potential to produce a higher energy storage density than state of the art batteries. A recently articulated goal by NASA[7] is to achieve an energy storage density of 400 Wh/kg.

G. Chemical

The most familiar energy storage device is the battery. There are two general categories of batteries, primary and secondary. For the purpose of persistence, only secondary, i.e. rechargeable, batteries are of interest. There are a wide variety of possibilities, but among the highest specific energy capacity are the Li-ion batteries that may reach a specific energy density of approximately 200 Wh/kg. In view of the well developed technology for such devices, they are obviously attractive, but are somewhat marginal, for the purpose of low mass, long duration power.

H. Thermal Energy Storage

The figure below compares the specific energy storage available via a number of alternatives for both thermal energy storage and rechargeable electric battery energy storage.

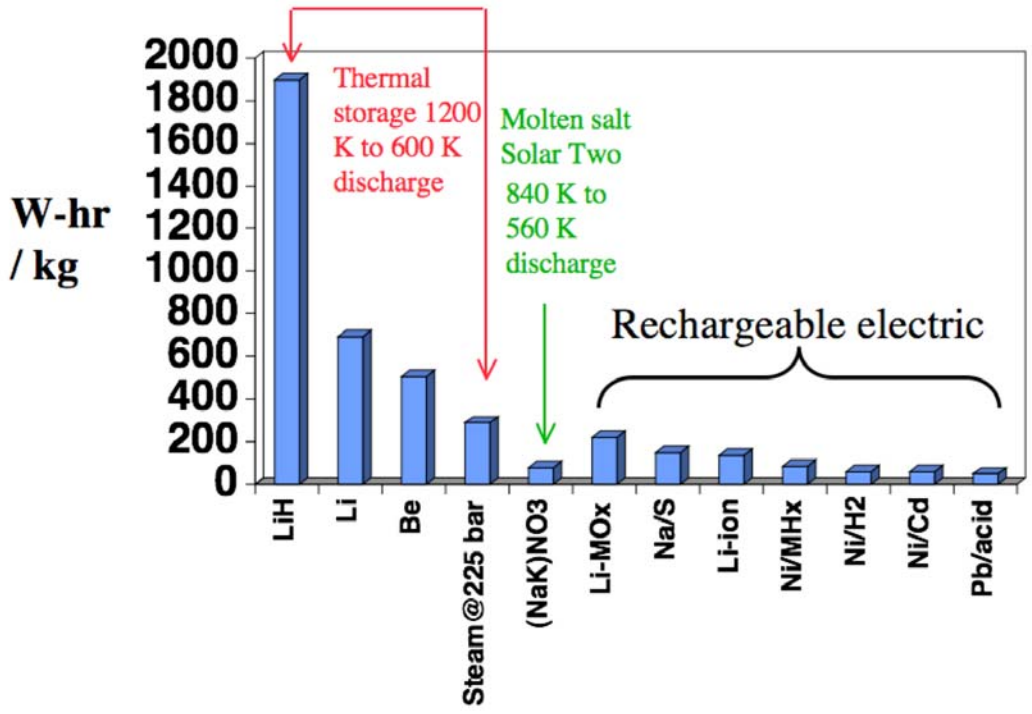

Figure 10. The specific energy content of various thermal energy storage systems and a number of electrical energy storage systems are compared.

Although pure hydrogen gas would have a thermal energy storage density of approximately 2,500 Wh/kg over the 600 K temperature range assumed for the cases in the plot above, since gaseous hydrogen must be contained in a pressure vessel, the mass of the vessel greatly dominates its specific energy storage.

Among all known alternatives, the thermal energy storage density of LiH is the highest, and indeed exceeds the energy storage density of rechargeable electric batteries by an order of magnitude.

A sine qua non of thermal energy storage systems for the purpose of power production is that the thermal energy must be converted to useful energy, either electrical, for most payload applications, or for propulsion. Especially in the context of a high altitude aircraft, the availability of very low temperature air enables more efficient heat engines than are practical in the terrestrial environment, as will be discussed in much greater detail below. However, in the next section, we consider the case of thermal energy storage in LiH in greater detail, in order to understand its limitations and capabilities.

IV. Lithium Hydride Thermal Energy Storage

Lithium hydride is theoretically, after hydrogen itself, the second lightest molecule. As pointed out above, pure hydrogen would have the highest specific heat of any molecule, but with inclusion of the mass of the vessel required to contain the gas, the thermal energy storage density of the system of gas plus container is not high at all.

In qualitative terms, the fundamental reason that LiH is capable of storing so much thermal energy per unit mass is essentially that the highly reactive, light alkali Lithium metal keeps the partial pressure of the lightest molecule, Hydrogen, in check. In the following section, the nature of this phenomenon is described more quantitatively.

A. Phase Structure of LiH+Li Mixtures

The temperature composition phase diagram[8] for the system of LiH+Li is displayed in figure 11. The L_1 phase on the left hand side of the diagram, which is enriched with lithium, is arbitrarily distinguished from the L_2 phase on the right hand side, which is enriched with hydride. The horizontal boundary at about 700°C corresponds to a monotectic phase transition. Below the monotectic temperature and above the melting point of lithium at 180°C, a mixture of two phases, a very lithium rich liquid, and an essentially pure lithium hydride solid, is found. Above the monotectic temperature, in the region labeled L_1+L_2, an immiscible mixture of two liquid phases, is found. Because these two liquids are

immiscible and have a significant density difference, under quiescent conditions, the lighter L_1 phase tends to “float” on top of the heavier L_2 phase. As the temperature increases through the immiscible liquids region, some of the hydrogen bound in the L_2 phase dissociates, and by virtue of the much lower density of hydrogen gas, bubbles up through the L_1 phase and into a vapor space above the liquids. Thus, as the temperature increases, the equilibrium vapor pressure of hydrogen also increases.

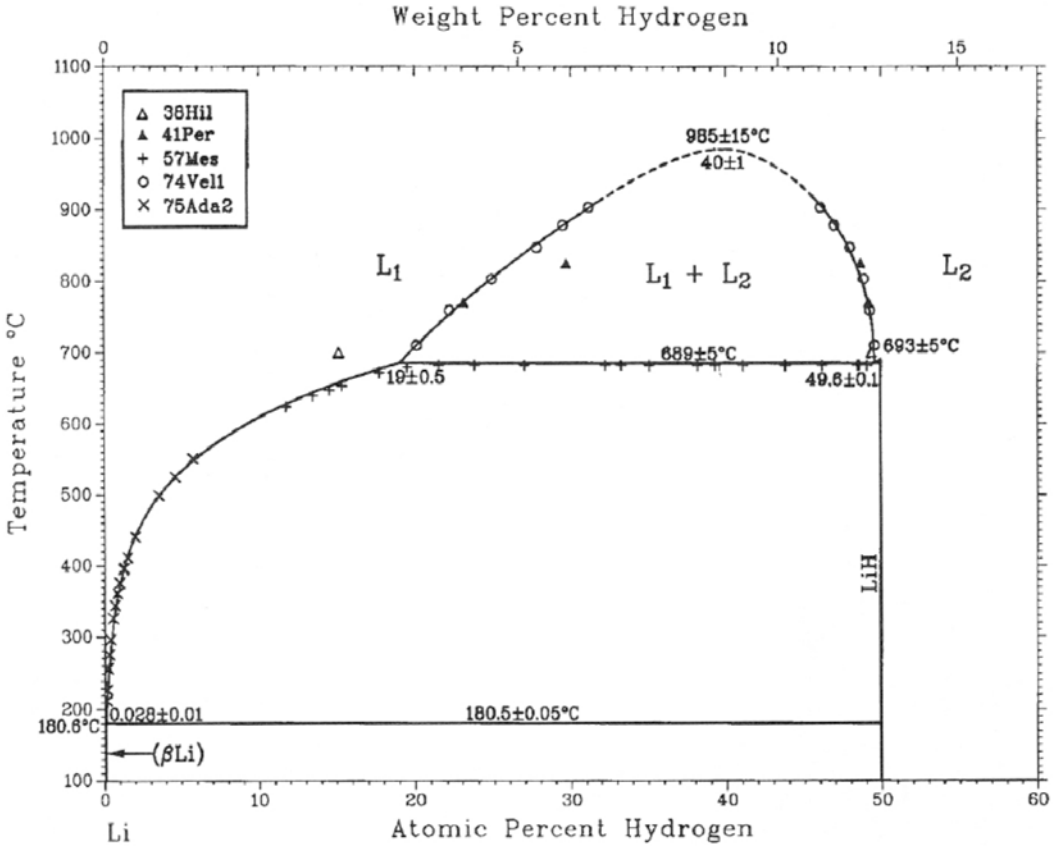

Figure 11. The phase diagram for mixtures of LiH and Li is displayed.

B. Lithium Hydride – Lithium Equilibrium with Hydrogen

As a mixture of LiH and Li is heated in a closed container, an equilibrium pressure of hydrogen gas is developed that depends on the relative quantity of lithium in the mixture. In general, the greater the lithium fraction, the lower the hydrogen pressure.

The horizontal sections of the curves displaying the equilibrium hydrogen vapor pressure values taken from Shpil'rain[9] in figure 12 correspond to the immiscible phase of the monotectic solution of LiH with Li. The behavior of a mixture of LiH + Li from which the hydrogen is continuously removed would be dynamic, and would depend on the temperature. As an example, consider a sample of pure LiH, initially at room temperature. The partial pressure of hydrogen in equilibrium with room temperature LiH is essentially zero, and thus very little hydrogen would be extractable from it. If the LiH is raised to 800 K, it will remain in the solid state, but will have a partial pressure of almost 100 Pa of hydrogen, and with continuous removal of the hydrogen, the Li fraction will gradually increase. Eventually, with sufficient removal of hydrogen, so that the mixture becomes almost pure Li, the partial pressure of hydrogen will decrease, as can be seen in the lowest curve in the figure.

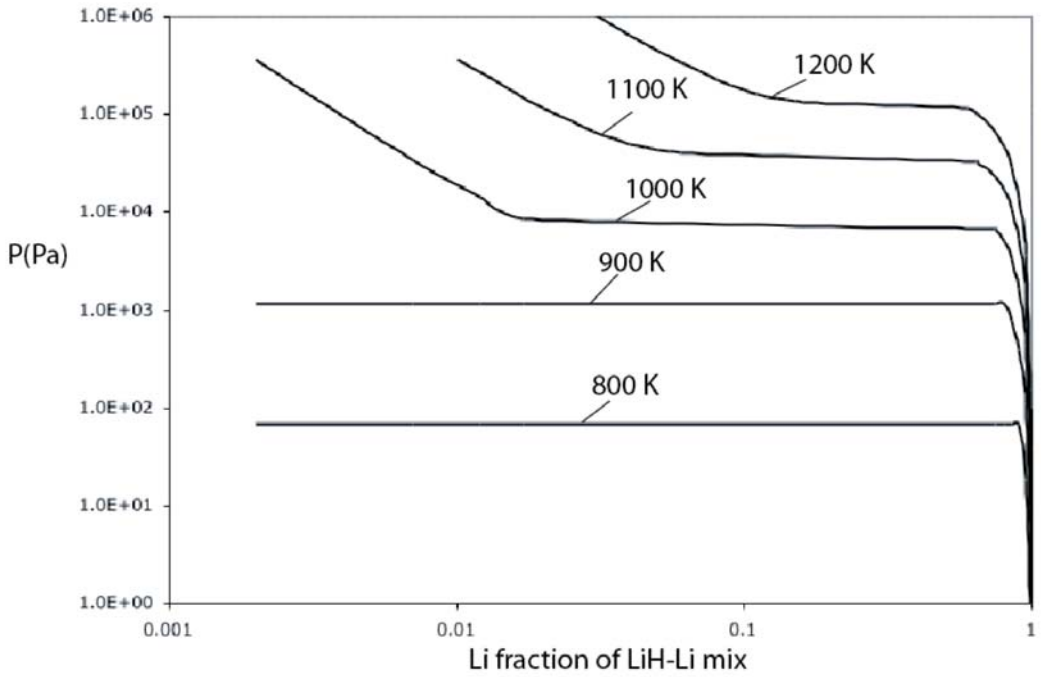

Figure 12. The partial pressure of hydrogen in equilibrium with a mixture of LiH and Li is plotted as a function of temperature.

A similar transformation occurs for any temperature below the melting point of LiH, at 973K. If the temperature is raised above the melting point, however, there is a qualitative difference in the behavior, since the vapor pressure of hydrogen becomes initially very high, until sufficient hydrogen is removed from the mixture to get to the horizontal portion of the appropriate curve, such as the examples shown in the above figure. Although theoretically the vapor pressure of hydrogen above a pure sample of LiH would be infinite above the melting point, as soon as some hydrogen is dissociated, the Li fraction becomes non-zero, and the equilibrium vapor pressure becomes a large, but finite, value.

This phenomenon of extremely large vapor pressure for pure LiH above the melting point is not merely academic, as a closed container of LiH salt that is rapidly heated will have a tendency to explode.

On the other hand, given a finite permeability to hydrogen through the walls of a container, the LiH fraction of a LiH+Li mixture will gradually decrease, and this will decrease the specific energy storage capability of the system.

Next consider an intermediate mixture of LiH + Li. Starting from an initial temperature well below the melting point of Li, all constituents of a sealed vessel are initially in the solid state. As the temperature is raised above 454 K, the lithium fraction in the mixture melts, and flows throughout the porous granular mass of essentially pure LiH. By a combination of convective and conductive heat transport means, externally supplied heating is very readily brought to bear throughout the vessel containing the LiH + Li mixture, and the solid LiH is very effectively brought up in temperature along with the liquid lithium. With further heating, and as portions of the solid LiH mass reach the melting point at 972 K, they tend to be immersed within a bath of very lithium rich liquid. Thus, although hydrogen gas is released from the LiH rich solid grains by dissociation, this gas quickly reacts with the surrounding liquid, and a mixture of two liquid phases is produced, a LiH rich fraction and a Li rich fraction, together with a dissolved portion of hydrogen gas, and a vapor pressure of hydrogen gas above the condensed matter at nearly the equilibrium partial pressure. Under quiescent

conditions, without vigorous “boiling” or cooling, or mechanical agitation, the LiH rich liquid phase is denser than the Li rich liquid phase, and it tends to settle to the bottom of the vessel.

With further heating, the LiH rich liquid on the bottom of the vessel “boils” off hydrogen gas. This hydrogen gas tends to rise quickly through the LiH rich liquid but as it passes into the Li rich liquid the hydrogen quickly re-combines with the Li rich liquid. As a result of such processes, a fairly vigorous convective stirring is produced, and the LiH+Li mixture tends to be effectively isothermalized.

C. Cooling Behavior of LiH+Li Mixture

For the purposes of supplying thermal energy to a given load, it is important to understand potential limitations on the rate of heating possible for any given thermal energy storage material. For this reason, the nature of the cooling process for potential thermal energy storage candidates is of great interest.

Fortunately, the behavior of a LiH+Li mixture on cooling turns out to have mechanisms that promote very effective heat transport. By virtue of the monotectic nature of the LiH+Li system, the LiH rich liquid fraction tends to freeze in a dendritic fashion, and produces a very porous structure. As a result, the Li rich fraction that remains liquid until very much lower temperature remains as a highly thermally conductive bath enveloping the LiH rich porous structure. The extraction of heat from the LiH+Li mixture can be at a very high rate, with only a modest temperature gradient.

We have quantified these limits in a series of cooling experiments with samples of LiH and Li at various mixture ratios. A representative example of data from these experiments is shown in figures 13 and 14.

In these measurements, test samples consisted of an iron cylinder, 1” diameter by 2” tall, filled with a mixture of LiH and Li in a glove box under an Argon atmosphere. These cylinders had open tops, and matching circular lids. Once filled with LiH and Li, the circular lids were loosely fit to the top of the cylinders, and the cylinders were transported to an electron-beam welding machine under Argon. In the e-beam welding machine, the samples were evacuated, and the circular lids were welded to the top of the cylinder to form a hermetically sealed container. Thermocouples were then welded to the side walls of the cylinder.

Figure 13 shows two images. On the left hand side is an ordinary radiograph of one of the test samples after going through a cycle of melting and freezing. The bright white vertical lines are the walls of the cylinder. The top lid and the cylinder bottom are just off scale to the top and bottom. A representative thermocouple sensor and leads are indicated in the figure. On the right hand side a Computed Tomography (CT) image of the same sample can is displayed. In this case, the bright wide solid vertical rectangular features correspond to the iron walls of the container. Outside the iron container one of the thermocouple leads can also be seen. The brighter portions of these images correspond to the denser regions of material. In the CT scan, a clear separation is seen between the most

dense iron material, labeled “Fe” in the figure, the intermediate density material, labeled “Li” in the figure, and the lowest density material, labeled “LiH” in the figure. From the x-ray opacity, the mean density of the LiH material is estimated to range between approximately 1/3 to ¼ of the theoretical density for solid LiH crystals. Although there is some fine scale “grainy” looking structure in the CT scan, it is not clear that the x-ray spatial resolution is really sufficient to identify this texture with the physical texture of the condensed LiH material. In any case, from the mean density alone, it is clear that the LiH material is very porous.

The thermal history of the material illustrated in figure 13 is as follows. With an electric band heater wrapped around the test cylinder, contained in a vacuum chamber, the samples were slowly heated to beyond the melting point of LiH. After sufficient time to assure that all of the LiH was molten, the heater was turned off and the sample allowed to cool, essentially entirely by radiation as there was only modest conductive cooling available. The time dependence of the temperature measured by the four thermocouple sensors is plotted in figure 14. In this case, the two thermocouples attached further from the middle of the sample displayed a somewhat lower temperature than those at the ends. As the sample cooled, the temperature curves display two plateau regions. The hotter plateau corresponds to the freezing of LiH, while the cooler plateau corresponds to the freezing of lithium. The temperature of the plateaus for the “closer” thermocouples differs by approximately 50°C from the melting point of LiH-Li,

while the temperature of the plateaus for the outer thermocouples differ by approximately 100°C from the LiH-Li melting point. This difference is associated with the finite thermal conduction, both through the LiH-Li material itself, and through the iron wall of the cylinder. Before and after each of the temperature plateaus, the rate of energy decrease in time of the LiH-Li material is easily quantified by the sample mass times the specific heat times the rate of decrease of the temperature vs. time. This thermal power loss estimate is in good agreement with simple black body radiation from the surface of the iron cylinders.

Table 2. Summary of LiH+Li Cooling Experiments

Substance	Melting Time (minutes)	Melt Temperature (K)	Heat of Fusion (W-hr/kg)	Thermal Power (W/kg)	Power Flux (W/m^2)
LiH	6	965	750	7500	$2.2x10^4$
Li	20	454	120	360	

From these measurements, together with the temperature drop between the freezing LiH and the neighboring thermocouples of 50°C, and neglecting the temperature drop contribution through the iron walls, the effective thermal conductivity corresponds to at least 400 $W/m^2/K$. For reference, this happens to be virtually equal to the conductivity of copper. In contrast the thermal conductivity of solid LiH is less than 5 $W/m^2/K$, while liquid lithium is about 50 $W/m^2/K$ at 800 K. It is clear from this data that the heat transport is an order of magnitude larger than would be supported by purely conductive transport alone. It

is also inferred from the general dendrictic freezing nature of the monotectic mixtures, together with the high porosity LiH condensed state observed in figure 13, that quite active convective heat transport occurs in the freezing of LiH+Li mixtures of compositions near those in the present experiments.

D. Conclusions Concerning LiH+Li Mixtures for Thermal Energy Storage

Since the data acquired in the course of this project strongly supports the existence of vigorous convective heat transport via the liquid lithium bath that permeates through the highly porous lithium hydride solid material, there is good reason to expect that very effective heat transport would be enabled at much larger scales than the 1” characteristic size of the present experiments. We conclude that not only does LiH have the very high specific latent heat desirable for provision of heat to a solar powered high altitude aircraft, but it also has a very favorable heat transport rate, with an effective thermal conductivity that rivals or exceeds that of copper.

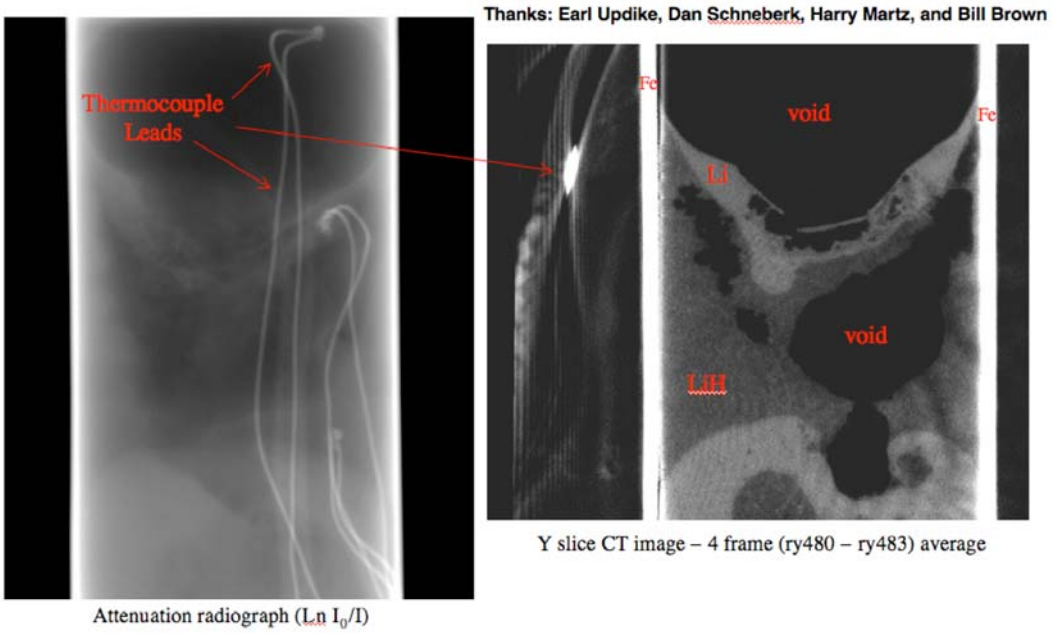

Figure 13. X-ray images

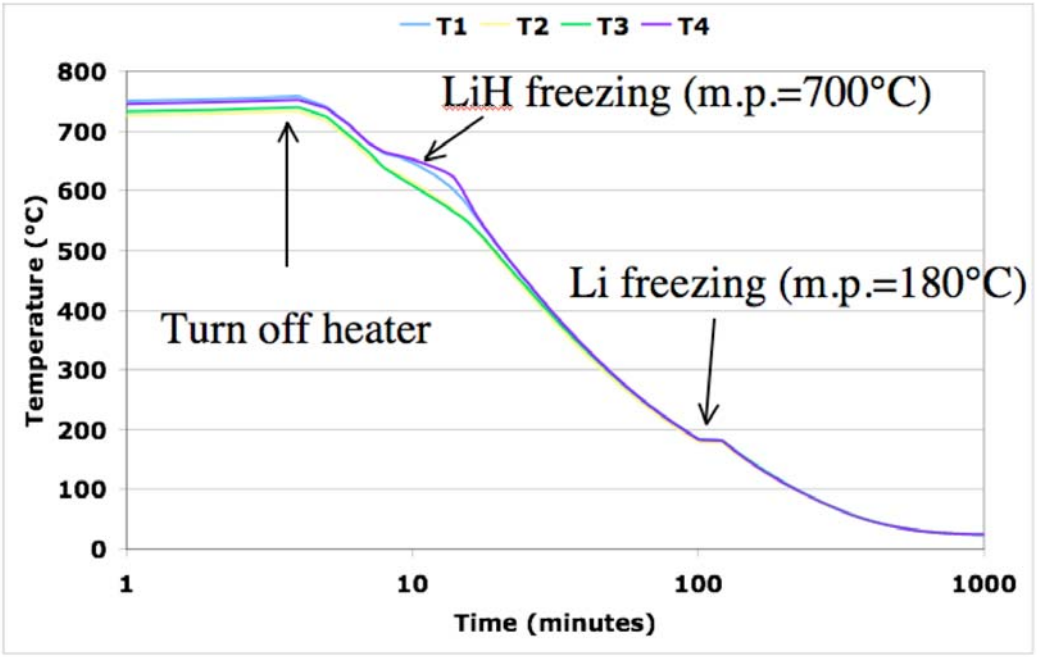

Figure 14. Cooling curves

V. Heat Engine Technology

As stated above, there is a great premium on the specific energy density for high altitude surveillance platforms. The use of thermal energy storage thus requires an efficient heat engine for the conversion of heat to propulsive power. Since electric power is so important in the modern world, there is a vast realm of knowledge and technology surrounding the production of electric power. It is most helpful to survey this knowledge base in order to quantify plausible heat engine efficiency levels relevant to the present solar powered aircraft study.

One recent study[10] is particularly helpful in this regard. The wide range of electric power generation systems considered in this report is listed in the following table in order of electric power generation efficiency. Many of these systems are not directly relevant to the present case of generation of power from thermal energy storage. However, those systems based on external combustion or other means of "external" heating are relevant, and are so noted in the table below.

It is noteworthy that almost all of the most efficient thermal power plants for the production of electricity involve very large scale turbomachinery, and most of these further involve a Rankine thermodynamic cycle. For example, the most efficient thermal power plants are based on the combustion of fuel in a gas turbine combined with a steam turbine powered by the steam generated from the gas turbine exhaust.

Table 3. Efficiency Comparison of Electric Power Plants

Power Plant Type	Practical Efficiency	External Combustion or Heating
Large Hydro	95%	
Small Hydro	90%	
Tidal	90%	
Combined Cycle Gas Turbine	58%	Y
Melted Carbonates Fuel Cell	52%	
Pulverised Coal Ultra Critical Steam	47%	Y
Solid Oxide Fuel Cell	46%	
Integrated Coal Gasification Combined Cycle	43%	
Circulating Fluidized Bed Combustion	40%	Y
Pressurised Fluidized Bed Combustion	40%	Y
Biomass Gasification Combined Cycle	40%	Y
Proton Exchange Membrane Fuel Cell	40%	
Large Gas Turbine	40%	
Steam Turbine, Coal Fired	43%	Y
Steam Turbine, Fuel Oil	41%	Y
Wind Turbine	35%	
Nuclear	35%	
Biomass	30%	Y
Waste to Electricity	25%	Y
Diesel Combined Heating Power (power only)	30%	Y
Solar Dish Stirling	20%	Y
Small & Micro-Turbines	19%	
Photo-Voltaic Cells	15%	
Geothermal Power	15%	Y
Solar Parabolic Trough	16%	Y
Solar Power Tower	16%	Y

Since the power levels of interest for a solar powered aircraft are in fact quite modest, the technology of large scale stationary power plants does not seem to be appropriate for this purpose. Indeed, although the largest turbines can achieve an efficiency of 95%, as in the large hydro case, small and micro-turbines achieve

only 20% thermal efficiency. There is another aspect of Rankine cycle based power plants that is not well suited to the high altitude solar thermal aircraft. This is the fact that working fluids for Rankine cycle engines have very well defined critical points directly determined by the phase of the working fluid. For example, it is not feasible to use a steam engine below the freezing point of water at 273 K, while it becomes technically very challenging to greatly surpass the critical point at 220 bar and 647 K for water. It is thus not feasible to use water in a Rankine cycle and take advantage of the ambient temperature in the stratosphere of approximately 220 K. Other phase change working fluids have similar temperature range limitations. As another example, although ammonia would remain liquid at stratospheric temperature, its critical point is only 407 K, and it is not feasible to take advantage of the much higher melting point of Lithium Hydride at 970 K for heating a Rankine cycle based on ammonia.

In examining the systems in the above table that do have a unit power scale that is more appropriate for a solar powered aircraft, and are amenable to a much broader span of temperatures appropriate for the high altitude environment, the Solar Dish Stirling case stands out. From the above table, Solar Stirling Dish systems, in current practice, seem to have an undesirably low efficiency. However, most of the contributions to the poor efficiency for Solar Dish Stirling systems listed in the table above are the result of losses in the collection of solar energy, but not in the conversion of heat to power. Furthermore, the stationary applications to solar

power plants are not able to take advantage of the low temperature reservoir of the stratosphere.

A. Stirling Engine Technology

The most efficient solar thermal power plants on the ground are currently based on Stirling engines located at the focus of a parabolic dish solar concentrating mirror. A recent overview[11] summarizes the state of the art of these systems. The most efficient among all of the Stirling Dish systems discussed has a Stirling engine with a thermal efficiency of 41% for the engine alone.

Results from another recent comparison of existing Stirling engine efficiencies are displayed in figure 15. Here the thermal efficiencies relative to the theoretical Carnot limiting efficiency are plotted as a function of the ratio of the heater temperature to the cooler temperature. It can be seen that this ratio lies between 45% and 65% for the range of engines displayed. It is also apparent that the efficiencies for real Stirling engines relative to the Carnot efficiency, tend to increase significantly with a greater hot to cold temperature ratio. Note that this is in addition to the increase in efficiency associated with the Carnot factor itself.

In extrapolating to the case of a Stirling engine used in a high altitude aircraft, with access to cooling at 220 K, and heating at the melting point of LiH, at 960 K, corresponding to a temperature ratio of 4.36, it is not unreasonable to estimate that at least 2/3 of the Carnot limit efficiency may be attained. This would be a thermal efficiency of over 50%.

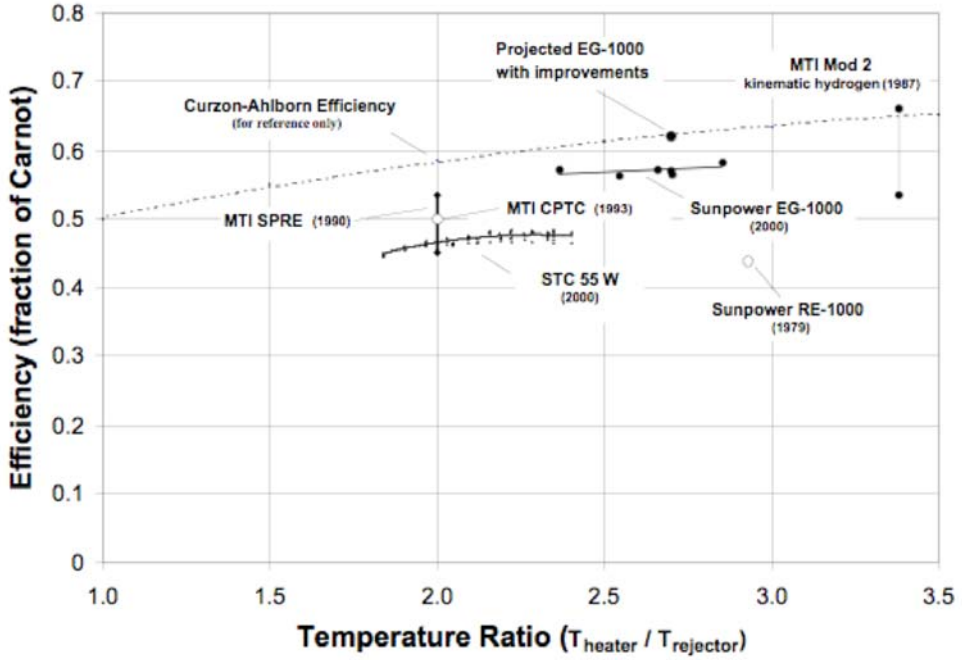

Figure 15. The efficiency for a number of actual Stirling engines relative to the ideal Carnot efficiency is plotted as a function of the hot to cold absolute temperature ratio. This figure is taken from Wood and Lane[12].

In addition to the thermal efficiency, another important aspect of the power plant is the power to mass ratio of the heat engine itself. The best guide for what can be done is based on a comparison of the power vs. mass for existing engines. In figure 16, three Stirling engines are represented, two made by Sunpower, and the third, an engine studied as part of the Automotive Stirling Engine, ASE study. It can be seen that the power to mass ratio varies nearly linearly (1 kg per 100 W) over three orders of magnitude in power.

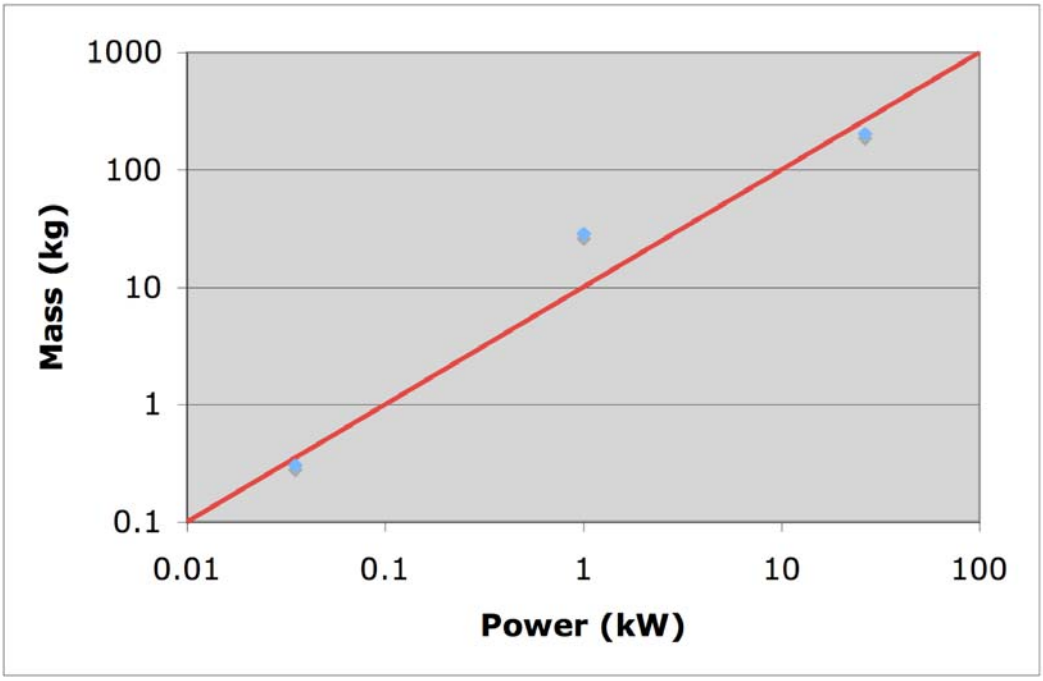

Figure 16. The mass of various Stirling engines is plotted as a function of their output power rating.

B. Heat Engine Summary and Conclusions

Taking the power to mass scaling found in real Stirling engines, together with a plausible deployed thermal efficiency of 50% in the stratospheric environment, a 1 kW power plant requires 2 kW of thermal power. For a 12 hour storage duration, the thermal energy storage requirement is 24 kWh. Assuming LiH as the storage medium, this requires approximately 12 kg of LiH. This is very nearly the same mass as the engine itself, leading to a total of engine plus thermal energy

storage medium mass of 20 to 25 kg per kW, or alternatively, a specific power level of 40 to 50 W/kg. Since the mean thrust power to displaced air mass ratio for a Lutz-Wagner airship was only a few W/kg, it does seem feasible to devote approximately 10% of the airship mass to the powerplant.

VI. Patents Pending

As a direct result of the research and development work pursued in the course of this project, several pending patents have been produced. These include those listed in the following table.

Pending Patents Produced in this Project

Invention Title	ROI#	Date	Current Status
Solar Thermal Aircraft	IL-11130	1/24/2003	PTO allowed: patent to issue
Year-Round Solar Thermal Power	IL-11474	1/14/2005	On LLNL patent priority list
Harmonic Engine	IL-11606	12/12/2005	To be filed 2/2007
Improved Ericsson Engine	IL-11633	2/8/2006	To be filed 3/2007
Residential Solar Thermal Power Plant	IL-11687	4/27/2006	Application filed 10/4/2006
Solar Siphoning Steam Power	IL-11742	10/16/2006	On LLNL patent priority list
Self-pressurizing Stirling Engine	IL-11130 divisional		Application filed 2/23/2007

While these patents are pending, enabling details will not be published, and are not included here. Several companies have expressed a great deal of interest in the technology represented by the above portfolio, and licensing negotiations are currently underway.

VII. Conclusion

In conclusion, it does appear that thermal energy storage coupled with an efficient heat engine is a viable approach for the provision of a high altitude platform that can remain aloft for an indefinitely long period of time.

VIII. Acknowledgements

The personnel involved in this project has varied throughout the course of this work. The individuals that have contributed to this project have included, in one form or another, in alphabetical order:
Omar Bashir, Marina Bastea, Harry Brandt, Preston Carter, Wilburt Davis, Moe Dehghani, Doug Dobie, Jim Emig, Mark Gauthier, Tom Gorman, Allen House, Will Hunt, Dick Landingham, Jenny Pruneda, Ray Smith, Chris Spadaccini, Pete Tirapelle, Ethan Welty, Case Van Dam, and Kipp Whittaker.

This work was performed under the auspices of the U.S. Department of Energy by University of California, Lawrence Livermore National Laboratory under Contract W-7405-Eng-48.

References

[1] This figure is from http://www.sanswire.com/operationalrequirements.html

[2] The radiosonde observations were taken from the NASA web-site: daaac.gsfc.nasa.gov.

[3] This animation is taken from http://svs.gsfc.nasa.gov/vis/a000000/a003200/a003203/

[4] T. Lutz and S. Wagner, "Drag reduction and shape optimization of airship bodies", AIAA Lighter-Than-Air Systems Technology Conference No. 12, San Francisco, CA (1997)

[5] See for example: http://en.wikipedia.org/wiki/Flywheel_energy_storage

[6] See for example: http://en.wikipedia.org/wiki/Supercapacitor

[7] K.A. Burke, "Unitized Regenerative Fuel Cell System Development", report no. NASA TM-2003-212739 (2003)

[8] F.D. Manchester, ed. "PHaseDiagrams of Binary Hydrogen Alloys", from the Monograph Series on Alloy Phase Diagrams, pub. ASM International, Materials Park, OH, (2000) p. 75

[9] E.E. Shpil'rain, K.A. Yakimovich, T.N. Mel'nikova, and A. Ya. Polishchuk, "Thermophysical Properities of Lithium Hydride, Deuteride, and Tritide and of Their Solutions with Lithium", translated by S.J. Amoretty, American Institue of Physics translation series, AIP, N.Y. (1987)

---

[10] "Efficiency in Electricity Generation", report drafted by EURELECTRIC "Preservation of Resources" Working Group's "Upstream" Sub-Group in collaboration with VGB PowerTech, July 2003

[11] T. Mancini, P. Heller, B.Butler, B. Osborn, W. Schiel, V. Goldberg, R. Buch, R. Diver, C. Andraka and J. Moreno, "Dish-Stirling Systems: An Overview of Development and Status", Journal of Solar Energy Engineering, May 2003, 125, pp. 135

[12] J.G. Wood and N. Lane, "Advanced 35 W Free-Piston Stirling Engine for Space Power Applications", from the proceedings of the 2003 STAIF conference.